Decoupling P-NARX models using filtered CPD

Jan Decuyper * **David Westwick** ** **Kiana Karami** ***
Johan Schoukens *,****

* *Department of Engineering Technology, Vrije Universiteit Brussel,
Pleinlaan 2, 1050 Brussels, Belgium (e-mail: jan.decuyper@vub.be,
johan.schoukens@vub.be)*
** *Department of Electrical and Computer Engineering, University of
Calgary, Calgary, Canada (e-mail: dwestwic@ucalgary.ca)*
*** *Department of Electrical Engineering and Electrical Engineering
Technology, Penn state Harrisburg, Middletown, PA, USA, 17057
(e-mail: kfk5551@psu.edu)*
**** *Department of Electrical Engineering, Eindhoven University of
Technology, Eindhoven, The Netherlands*

Abstract: Nonlinear Auto-Regressive eXogenous input (NARX) models are a popular class of
nonlinear dynamical models. Often a polynomial basis expansion is used to describe the internal
multivariate nonlinear mapping (P-NARX). Resorting to fixed basis functions is convenient since
it results in a closed form solution of the estimation problem. The drawback, however, is that
the predefined basis does not necessarily lead to a sparse representation of the relationship,
typically resulting in very large numbers of parameters. So-called decoupling techniques were
specifically designed to reduce large multivariate functions. It was found that, often, a more
efficient parameterisation can be retrieved by rotating towards a new basis. Characteristic
to the decoupled structure is that, expressed in the new basis, the relationship is structured
such that only single-input single-output nonlinear functions are required. Classical decoupling
techniques are unfit to deal with the case of single-output NARX models. In this work, this
limitation is overcome by adopting the filtered CPD decoupling method of Decuyper et al.
(2021b). The approach is illustrated on data from the Sliverbox benchmark: measurement data
from an electronic circuit implementation of a forced Duffing oscillator.

Keywords: Polynomial-NARX, decoupling, filtered CPD, model reduction, nonlinear system
identification

1. INTRODUCTION

Nonlinear auto-regressive exogenous input (NARX) models have been extensively used to describe nonlinear systems. It is a black-box system identification technique which has proven to be useful in a wide range of applications (Chan et al., 2015; Zhao et al., 2013). NARX models describe dynamical nonlinear behaviour by relating the current output sample to both past output samples, and current and past input samples. Defining

$$\boldsymbol{x} = \{u(t), u(t-1), \dots, u(t-n_u),$$
$$y(t-1), \dots, y(t-n_y)\}, \qquad (1)$$

a general single-output NARX model is described by (Billings, 2013)

$$y(t) = F(\boldsymbol{x}) + e(t), \qquad (2)$$

where $F : \mathbb{R}^{n_u + n_y + 1} \to \mathbb{R}$ is a static multiple-input single-output (MISO) nonlinear function and $e(t)$ is an equation error which is assumed to be a sequence of independent identically distributed (IID) random variables. The function F may be described by any class of functions, e.g.

it can be a neural network or a wavelet network. Often, however, a basis expansion is preferred. In that case, a direct estimate of the model parameters follows from linear regression by using the measured outputs in the regressor (minimising the equation error). A popular choice is the polynomial basis, leading to so-called Polynomial-NARX or P-NARX models.

The ease of identification is however countered by a number of fundamental disadvantages. P-NARX models are notorious for the number of parameters that have to be identified, growing both with the number of past inputs and past outputs, $n = n_u + n_y + 1$, and combinatorially with the nonlinear degree d. Moreover, being a black-box method, the obtained model is often very hard to interpret. General practice is to use regularisation to steer the optimisation towards meaningful terms and hence reduce the number of parameters. Often, however, no sparse representation can be obtained using the classical monomial basis. The present work promotes the use of decoupling techniques, which were designed to translate the relationship into a more favourable basis.

Similar issues have already been addressed in the context of nonlinear state-space models, where typically

a multiple-input multiple-output (MIMO) polynomial is used to describe the nonlinearity. It was found that by *decoupling* the multivariate polynomial into a number of univariate polynomials, both insight and model reduction could be obtained (Decuyper et al., 2021a).

In general, decoupling techniques aim at transforming generic multivariate nonlinear functions into decoupled functions. The decoupled structure is characterised by the fact that the nonlinear relationship is described by a number of univariate functions of intermediate variables. Given a generic nonlinear function

$$\boldsymbol{q} = \boldsymbol{f}(\boldsymbol{p}) \tag{3}$$

with $\boldsymbol{q} \in \mathbb{R}^m$ and $\boldsymbol{p} \in \mathbb{R}^n$, the idea is to introduce an appropriate linear transformation of $\boldsymbol{p}$, denoted $\boldsymbol{V}$, such that in this alternative basis, univariate functions may be used to describe the nonlinear mapping. The decoupled function is then of the following form

$$\boldsymbol{f}(\boldsymbol{p}) = \boldsymbol{W}\boldsymbol{g}(\boldsymbol{V}^{\mathrm{T}}\boldsymbol{p}) \tag{4}$$

where the ith function is $g_i(z_i)$ with $z_i = \boldsymbol{v}_i^{\mathrm{T}}\boldsymbol{p}$, emphasising that all functions are strictly univariate. The number of allowed univariate functions, denoted r, is a user choice which can be used to control the model complexity. In some cases prior knowledge of the system may dictate that a certain number of nonlinear components drive the nonlinearity. Whenever no such knowledge is available, a scan over r is performed. The number of univariate functions plays a crucial role since it will determine whether the implied equivalence of Eq. (4) exists. A second linear transformation $\boldsymbol{W}$, maps the function back onto the outputs. The linear transformations then have the following dimensions: $\boldsymbol{V} \in \mathbb{R}^{n \times r}$ and $\boldsymbol{W} \in \mathbb{R}^{m \times r}$.

The original decoupling procedure requires the function to be of the MIMO-type (Dreesen et al., 2015), i.e $m > 1$, excluding the class of single-output P-NARX models. The method is based on the canonical polyadic decomposition (CPD) of a 3-way tensor, constructed out of evaluations of the Jacobian matrix along a number of operating points (see Section 3.2). It exploits the uniqueness properties of the CPD in order to retrieve estimates of the univariate functions g_i. In Westwick et al. (2018), the issue with single-output functions was circumvented by resorting to evaluations of the Hessian, again retrieving a 3-way tensor. In practice, however, the uniqueness of the CPD is often not guaranteed (Decuyper et al., 2019), leading to very noisy estimates of g_i or its derivatives. As a solution, Karami et al. (2021) proposed to add polynomial constraints when factoring the Hessian. Accurate decoupled models could be obtained, although at the price of computing the Hessian.

In this work, the filtered CPD approach of Decuyper et al. (2021b) will be used. It acts on the basis of first order derivative information, avoiding the computation of the Hessian, and resorts to non-parametric soft constraints to ensure meaningful estimates of g_i are obtained.

2. FILTERED CPD DECOUPLING

The filtered CPD approach (F-CPD) links the original function to a decoupled function on the basis of its first order derivative information. The method relies on the underlying diagonal structure of the Jacobian (Eq. (5)),
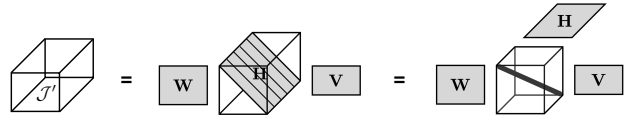

Fig. 1. Centre: a collection of evaluations of the Jacobian of the decoupled function (Eq. (4)), stacked in the third dimension. Left: the corresponding third order tensor, Right: extracting the central diagonal plane reveals a diagonal tensor decomposition.

which follows from the use of univariate functions g_i. Denoting the left and right hand side Jacobian of Eq. (4) by $\boldsymbol{J}$ and $\boldsymbol{J}'$, respectively, we have that

$$\boldsymbol{J}' = \boldsymbol{W} \operatorname{diag}\left(\begin{bmatrix} h_1(z_1) & \cdots & h_r(z_r) \end{bmatrix}\right) \boldsymbol{V}^{\mathrm{T}} \tag{5}$$

in which case $h_i(z_i) := \frac{dg_i(z_i)}{dz_i}$ represents the derivative of the univariate function $g_i(z_i)$ with respect to its argument. Evaluating this Jacobian in N operating points, i.e. for $\{\boldsymbol{p}[1], \cdots, \boldsymbol{p}[N]\}$, and collecting the evaluations in a third dimension, expands the object into a three-way array $\mathcal{J}' \in \mathbb{R}^{n \times m \times N}$. This is illustrated graphically in Fig. 1. Notice that the diagonal plane, $\boldsymbol{H} \in \mathbb{R}^{N \times r}$, stores evaluations of h_i, i.e the derivative of the functions g_i. Given the diagonal form, the collection of Jacobians may be written as a sum of r outer products (or rank-one terms). Element-wise we have that,

$$\mathcal{J}'_{[s,k,l]} = \sum_{i=1}^{r} w_{si} \, v_{ki} \, h_{li}, \tag{6}$$

for $s = 1, \ldots, m$ and $k = 1, \ldots, n$ and $l = 1, \ldots, N$. A sum of rank-one terms defines a diagonal tensor decomposition (Kolda and Bader, 2009). The latter is illustrated on the right in Fig. 1.

Dreesen et al. (2015) found that the underlying diagonal form of $\mathcal{J}'$ can be exploited in the decoupling process. It was suggested to construct a third order tensor, $\mathcal{J}$, out of evaluations of the Jacobian of the known function, $\boldsymbol{f}(\boldsymbol{p})$, and compute a diagonal decomposition such that $\mathcal{J} \approx \mathcal{J}'$. In the filtered CPD approach, finite difference filters are introduced into the decomposition. This allows for the Jocobian tensor to be decomposed into the more convenient factors $\{\boldsymbol{W}, \boldsymbol{V}, \boldsymbol{G}\}$, where $\boldsymbol{G}$ stores evaluations of the univariate functions g_i.

The method of Decuyper et al. (2021b) can be summarised in three steps:

(1) Collect the Jacobian matrices of the known function, $\boldsymbol{J}$, and stack them into a three-way array, i.e. the Jacobian tensor $\mathcal{J} \in \mathbb{R}^{n \times m \times N}$.
(2) Factor $\mathcal{J}$ into $\{\boldsymbol{W}, \boldsymbol{V}, \boldsymbol{G}\}$ by computing a filtered diagonal tensor decomposition (F-CPD).
(3) Retrieve the functions, g_i, by parametrising the non-parametric estimates stored in $\boldsymbol{G}$.

At the core of the algorithm lies an alternating least-squares routine which iteratively updates $\boldsymbol{W}, \boldsymbol{V}$, and $\boldsymbol{G}$. Starting from a random initialisation [1] the following norm is progressively minimised

---

[1] The retrieved local minimum depends on the initialisation point. In this work, however, no significant impact of the initialisation was observed when tackling the benchmark problem of Section 3.

$$\underset{\boldsymbol{W},\boldsymbol{V},\boldsymbol{G}}{\arg\min} \ \|\mathcal{J} - [\![\boldsymbol{W},\boldsymbol{V},\mathcal{F}_C(\boldsymbol{V})\circ\boldsymbol{G}]\!]\|_F^2, \qquad (7)$$

where the shorthand notation $\mathcal{J}' = [\![\boldsymbol{W},\boldsymbol{V},\mathcal{F}_C(\boldsymbol{V})\circ\boldsymbol{G}]\!]$ is used and '∘' defines a matrix-column product, illustrated by Eq. (9). In this formulation, $\mathcal{F}_C \in \mathbb{R}^{N\times N\times r}$ stores a collection of *finite difference filters*, with the ith filter

$$\boldsymbol{F}_{C_i} \coloneqq \mathcal{F}_{C_{[:,:,i]}}. \qquad (8)$$

A finite difference filter is a matrix which upon multiplication with a vector of function evaluations, returns a finite difference approximation. Recall that the ith column of $\boldsymbol{H}$ stores evaluations of the derivative of g_i with respect to $z_i = \boldsymbol{v}_i^{\mathrm{T}}\boldsymbol{p}$, resulting in the dependency $\mathcal{F}_C(\boldsymbol{V})$. We may then express $\boldsymbol{h}_i$, as the finite difference of the ith column of $\boldsymbol{G}$,

$$\boldsymbol{h}_i \coloneqq \boldsymbol{F}_{C_i}\boldsymbol{g}_i. \qquad (9)$$

The subscript C denotes that a central differencing scheme is used.

Eq. (7) can be broken down into 3 separate objectives, i.e. Eq. (10), (11), and (12). Denoting the matricisations of $\mathcal{J}$ along its rows, columns and tubes by $\boldsymbol{J}_{(1)}, \boldsymbol{J}_{(2)}, \boldsymbol{J}_{(3)}$, respectively, and using '⊙' to denote the Khatri-Rao product, an update of $\boldsymbol{W}$ is found from

$$\underset{\boldsymbol{W}}{\arg\min} \ \|\boldsymbol{J}_{(1)} - \boldsymbol{W}((\mathcal{F}_C(\boldsymbol{V})\circ\boldsymbol{G})\odot\boldsymbol{V})^{\mathrm{T}}\|_F^2 \qquad (10)$$

Given that $\boldsymbol{W}$ appears linearly in the objective, a closed-form update formula may be obtained.

What is imperative is to retrieve meaningful estimates of the functions g_i along the columns of $\boldsymbol{G}$. Originally one relied on the uniqueness properties of the CPD to meet this requirement (Dreesen et al., 2015). As was mentioned earlier, it has been shown that this uniqueness is often not guaranteed, leading to very noisy estimate.

The F-CPD method, on the other hand, relies on finite difference filters to steer the decomposition towards meaningful factors. What is required in practice is to promote smoothness on the estimates stored in $\boldsymbol{G}$. Given that both $\boldsymbol{V}$ (via $z_i = \boldsymbol{v}_i^{\mathrm{T}}\boldsymbol{p}$) and $\boldsymbol{G}$ contribute to the smoothness of the estimates of $g_i(z_i)$, a smoothness objective should be reflected in both their cost functions. Regularisation is used to penalise noisy estimates. An update of $\boldsymbol{V}$ is found from

$$\underset{\boldsymbol{V}}{\arg\min} \ \|\boldsymbol{J}_{(2)} - \boldsymbol{V}((\mathcal{F}_C(\boldsymbol{V})\circ\boldsymbol{G})\odot\boldsymbol{W})^{\mathrm{T}}\|_F^2 \\ + \lambda\|(\mathcal{F}_L(\boldsymbol{V})\circ\boldsymbol{G}) - (\mathcal{F}_R(\boldsymbol{V})\circ\boldsymbol{G})\|_F^2 \qquad (11)$$

where λ is a hyperparameter which balances both objectives. The additional term penalises divergent results from a left ($\mathcal{F}_L$) and a right ($\mathcal{F}_R$) finite difference filtering operation, ultimately steering the optimisation towards smooth solutions. Given that $\boldsymbol{V}$ appears nonlinearly in Eq. (11), nonlinear optimisation is required when computing an update.

In analogy with Eq. (11), the update formula of $\boldsymbol{G}$ is also found from a joint objective function.

$$\underset{\boldsymbol{G}}{\arg\min} \ \|\boldsymbol{J}_{(3)} - (\mathcal{F}_C(\boldsymbol{V})\circ\boldsymbol{G})(\boldsymbol{V}\odot\boldsymbol{W})^{\mathrm{T}}\|_F^2 \\ + \lambda\|(\mathcal{F}_L(\boldsymbol{V})\circ\boldsymbol{G}) - (\mathcal{F}_R(\boldsymbol{V})\circ\boldsymbol{G})\|_F^2 \qquad (12)$$

It can be shown that $\boldsymbol{G}$ appears linearly in Eq. (12).

The smoothness objective ensures that the functions may be parameterised using an appropriate basis expansion.

What basis expansion to use depends on the application and can be freely chosen by the user.

The computational cost of the algorithm is quadratic in both N and r. More efficient implementations are the subject of future study. For now, the benchmark problem of Section 3 could be solved in a computing time in the order of minutes. The present algorithm can be summarised by the following pseudocode.

F-CPD Algorithm
Construct Jacobian tensor $\mathcal{J}$
Randomly select N points from the input space $\{\boldsymbol{p}[k]\}_{k=1}^N$
Compute $\boldsymbol{J}_k$ on the operating points $\{\boldsymbol{p}[k]\}_{k=1}^N$
Stack the Jacobian matrices $\mathcal{J}[:,:,k] \coloneqq \boldsymbol{J}_k$
Factor $\mathcal{J}$ into $\{\boldsymbol{W},\boldsymbol{V},\boldsymbol{G}\}$
Initialise $\boldsymbol{W},\boldsymbol{V},\boldsymbol{G}$ for chosen value of r
Repeat ALS routine
update $\boldsymbol{W},\boldsymbol{V},\boldsymbol{G}$ via (10) to (12)
Until maximum number of iterations
Parameterise $\boldsymbol{G}$
obtain $g_i(z_i)$ from appropriate basis expansion of $\boldsymbol{G}$

The filtered CPD approach is a powerful tool since it no longer relies on the uniqueness properties of the CPD. As a result, the number of univariate functions, r, to be used in the decoupled function, has become a design choice.

Moreover, also multiple-input single-output functions, may be decoupled using filtered CPD. MISO functions result in Jacobian matrices rather than tensors, preventing the possibility of exploiting the uniqueness properties of the CPD. F-CPD therefore enables the decoupling of single-output NARX models, and by extent of general MISO functions.

3. BENCHMARK PROBLEM

The decoupling of single-output P-NARX models will be demonstrated on a nonlinear benchmark data set of the forced duffing oscillator. The data is obtained from an electrical implementation of a mechanically resonating system involving a moving mass m, a viscous damping c and a nonlinear spring $k(y(t))$. The analogue electrical circuitry generates data close to but not exactly equal to the idealised representation given by the nonlinear ordinary differential equation (ODE)

$$m\ddot{y}(t) + c\dot{y}(t) + k(y(t))y(t) = u(t), \qquad (13)$$

where the presumed displacement, $y(t)$, is considered the output and the presumed force, $u(t)$, is considered the input. Overdots denote the derivative with respect to time. The static position-dependent stiffness is given by

$$k(y(t)) = \alpha + \beta y^2(t), \qquad (14)$$

which can be interpreted as a cubic hardening spring.

The training data consists of 9 realisations of a random-phase odd multisine. The period of the multisine is $^1/f_0$ with $f_0 = {}^{f_s}/_{8192}$ Hz and $f_s \approx 610$ Hz. The number of excited harmonics is $L = 1342$ resulting in an $f_{\max} \approx 200$ Hz. Each multisine realisation is given a unique set of phases that are independent and uniformly distributed in $[0, 2\pi[$. The signal to noise ratio (SNR) at the output is estimated at approximately 40 dB. This is measurement noise (or sensor noise). It is high levels of measurement noise can deteriorate the performance of NARX models (Schoukens et al., 2021). It is important to stress that

this inherent sensitivity is not removed by replacing the internal function by a decoupled one.

As **validation data** a filtered Gaussian noise sequence of the same band width and with a linearly increasing amplitude is used.

The data are part of three benchmark data sets for nonlinear system identification described in Wigren and Schoukens (2013). The approach will consist of 3 steps:

(1) Identify a P-NARX model on the basis of the training data.
(2) Decouple the NARX model using the F-CPD technique.
(3) Use a final optimisation to minimise the simulation error of the decoupled model.

3.1 Reference P-NARX model

Using the System Identification toolbox in MATLAB a P-NARX model is estimated with the following properties: $n_u = 1$, $n_y = 3$, and $d = 3$. All cross-term monomials where included leading to a model with 55 parameters. We will denote the P-NARX model by $f(\boldsymbol{x}) : \mathbb{R}^{n_u+n_y+1} \rightarrow \mathbb{R}$, with $\boldsymbol{x}$ as defined in Eq. (1), emphasising that the model is obtained by minimising the equation error (focus on prediction). As performance metric a relative root-mean-squared simulation error is used

$$e_{\mathrm{rms}} = \frac{\sqrt{\frac{1}{N} \sum_{k=1}^{N} \left(y[k] - y_s[k]\right)^2}}{\sqrt{\frac{1}{N} \sum_{k=1}^{N} y[k]^2}} \times 100 \qquad (15)$$

where y_s denotes the simulated output and N is the record length. The estimation process returns an accurate P-NARX model yielding a e_{rms} of 1.01% when simulating the validation data.

3.2 Decoupled P-NARX model

Given that using the F-CPD method, r, has become a design choice, we are able to scan over r and study the performance of the obtained decoupled models. Additionally, a scan over the hyperparameter λ is required. Besides the simulation error (Eq. (15)) we will also introduce a function approximation error,

$$e_f = \frac{\sqrt{\frac{1}{N} \sum_{k=1}^{N} \left(f(\boldsymbol{x}_o[k]) - f_d(\boldsymbol{x}_o[k])\right)^2}}{\sqrt{\frac{1}{N} \sum_{k=1}^{N} f(\boldsymbol{x}_o[k])^2}} \times 100 \qquad (16)$$

in which f_d represents the decoupled polynomial function,

$$f_d = \boldsymbol{w}^{\mathrm{T}} \boldsymbol{g} \left(\boldsymbol{V}^{\mathrm{T}} \boldsymbol{x}_o\right), \qquad (17)$$

and $\boldsymbol{x}_o$ are the operating points. In this case N refers to the number of operating points for which the decomposition is computed.

In order to ensure that the operating points cover the region of interest, they are selected on the basis of the training data. Simulating the training data using the P-NARX estimate f returns the collection $\boldsymbol{X}_T = \{\boldsymbol{x}_T[k]\}_{k=0}^{N_T}$, with $\boldsymbol{x}_T$ containing the simulated output samples

$$\boldsymbol{x}_T = \{u(t), u(t-1), \ldots, u(t-n_u),$$
$$y_s(t-1), \ldots, y_s(t-n_y)\}, \qquad (18)$$

and N_T denoting the training record length. The operating points are then drawn from the joint normal distribution,
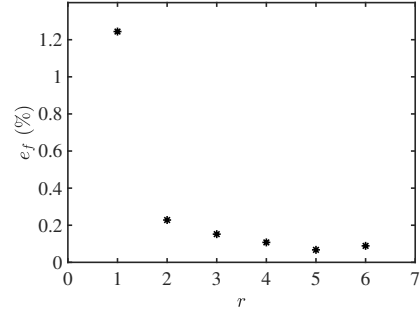

Fig. 2. Relative function approximation error computed on the operating points.

inferred from $\boldsymbol{X}_T$. The number of operating points to use can be considered a hyperparameter. In this work $N = 200$ points is used. In correspondence to the reference model, f, the functions g_i of the decoupled models will be parametrised using third order polynomials, $d = 3$.

We will study the decoupled models following the grid defined by $r = 1, \ldots, 6$ and $\lambda = 10^l$, with $l = -1, \ldots, 5$. For every value of r the decoupled model yielding the lowest function approximation error, e_f, is selected. This will correspond to the value of λ which results in the appropriate balance between the tensor approximation objective and the smoothness objective (Eq. (11) and (12)). The overview of the function approximation error is depicted in Fig. 2. Accurate function approximations, $f_d \approx f$, could be obtained yielding errors below 1% for values of $r > 1$.

In a final step, nonlinear optimisation is used to fine-tune the decoupled models on the basis of their training data simulation error. A Levenberg-Marquardt algorithm (Levenberg, 1944) is used to minimise the output error objective given by

$$\arg \min_{\boldsymbol{w}, \boldsymbol{V}, \boldsymbol{\theta}} \sum_{k=1}^{N_T} \left(y[k] - \boldsymbol{w}^{\mathrm{T}} \boldsymbol{g}(\boldsymbol{V}^{\mathrm{T}} \boldsymbol{x}_s[k], \boldsymbol{\theta})\right)^2, \qquad (19)$$

with y the true output, $\boldsymbol{x}_s$ containing simulated output samples of the decoupled model (similar to Eq. (18)), and $\boldsymbol{\theta}$ storing the coefficients of the third order polynomials in $\boldsymbol{g}$.

Fig. 3 illustrates the performance of the optimised model set when simulating the validation data. It is clear that decoupled models for which $r \geq 4$ perform equally well as the reference model, i.e $\approx 1\%$ (indicated by the red line). Models containing less univariate mapping functions miss the required complexity to reproduce the data up to such precision. For some applications, however, the performance of the $r = 2$ and $r = 3$ model may still be acceptable. The simulation performance of the $r = 4$ model is illustrated in Fig. 4.

Noticing that $\boldsymbol{w}$ merely serves as a scaling on the functions $\boldsymbol{g}$, the coefficients can be incorporated in $\boldsymbol{\theta}$. Doing so results in a total parameter count of 36 for the $r = 4$ model, compared to the 55 parameters required in the standard basis expansion of the reference model. The univariate functions of the decoupled model are depicted in Fig. 5. From visual inspection of the functions one may conclude that the system behaviour is dominantly cubic.
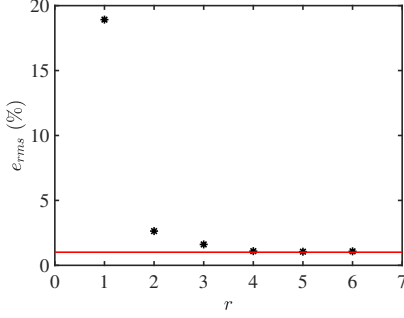
Fig. 3. Black markers: Relative simulation error of the decoupled P-NARX models, computed on the validation data. Red: error obtained from the reference P-NARX model.
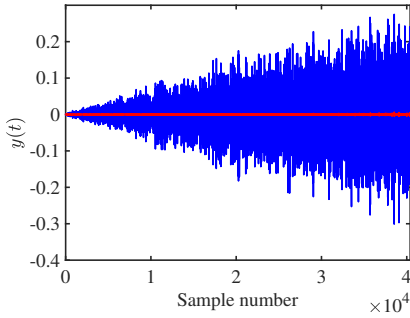

Fig. 4. Blue: validation output data corresponding to a filtered Gaussian noise sequence. The amplitude extends beyond the training data amplitude resulting in an extrapolation of the model. Red: simulation error of the $r = 4$ decoupled model.
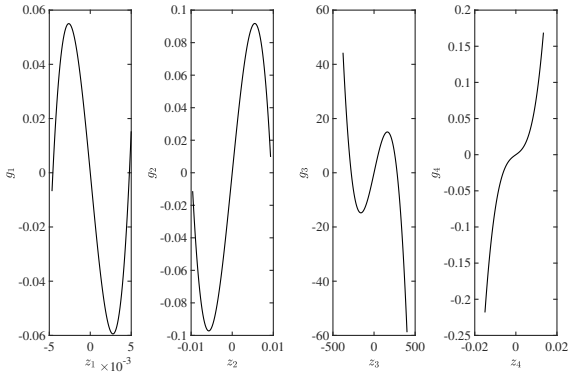

Fig. 5. Univariate functions of the $r = 4$ decoupled P-NARX model. The functions are evaluated over the validation range.

Additionally the SISO functions can easily be monitored to flag extrapolation (Karami et al., 2019). It should be noted that in this case, even after decoupling, physical interpretability remains hard. An important aspect is believed to be the choice of regressors, i.e. n_u, n_y. The use of shifted input samples contributes to retrieving a non-physical model, in this case of the forced Duffing oscillator. One such mechanism is the introduction of sampling zeros (Goodwin et al., 2013).

4. COMPARING POLYNOMIAL CONSTRAINTS TO F-CPD

In this section the decoupling technique of Karami et al. (2021), which will be referred to as the *the structured Hessian method*, is compared to the F-CPD method. Following the author's notation, the decoupled model may be written as

$$f_d = c_0 + \sum_{i=1}^{r} g_i(\boldsymbol{v}_i^{\mathrm{T}} \boldsymbol{x}) \tag{20a}$$

$$g_i(z_i) = \sum_{j=1}^{d} c_{j,i} z_i^j, \tag{20b}$$

which corresponds to Eq. (17) where $\boldsymbol{w}$ is incorporated in the vector of coefficients,

$$\boldsymbol{c} = [c_0\ c_{1,1}\ \ldots\ c_{d,1}\ c_{1,2}\ \ldots\ c_{d,r}]^{\mathrm{T}}. \tag{21}$$

Computing the Hessian of the output of the decoupled function with respect to the input variables generates a matrix for each operating point $\boldsymbol{x}_o$

$$\boldsymbol{H}_y'(\boldsymbol{x}_o) = \sum_{i=1}^{r} g_i''(\boldsymbol{v}_i^{\mathrm{T}} \boldsymbol{x}_o) \boldsymbol{v}_i \boldsymbol{v}_i^{\mathrm{T}} \tag{22}$$

where g_i'' denotes the second derivative of g_i with respect to z_i. The collection of Hessian matrices may again be stacked into a three-way array whose entries are given by

$$\mathcal{H}_{[j,k,l]}' = \sum_{i=1}^{r} v_{ij}\ v_{ik}\ g_{il}'' \tag{23}$$

for $j = 1, \ldots, n$ and $k = 1, \ldots, n$ and $l = 1, \ldots, N$.

The idea is to construct the Hessian tensor $\mathcal{H}$ out of evaluations of the known function and use the CPD to factor it into $\mathcal{H}' = [\![\boldsymbol{V}, \boldsymbol{V}, \boldsymbol{G}'']\!]$, such that $\mathcal{H} \approx \mathcal{H}'$. In this case $\boldsymbol{G}'' = [\boldsymbol{g}_1'' \ldots \boldsymbol{g}_r'']$ is a matrix storing evaluations of the second derivate of $\boldsymbol{g}$.

From the previous it is clear that relying on the uniqueness properties of the CPD alone does not guarantee to obtain accurate estimates of g_i''. It was therefore proposed not to solve for $\boldsymbol{G}''$ directly, but to formulate the matrix factor into a polynomial form and solve for the polynomial coefficients instead. The optimisation problem to be solved can be formulated as

$$\arg\min_{\boldsymbol{V},\boldsymbol{c}} \|\mathcal{H} - [\![\boldsymbol{V}, \boldsymbol{V}, \boldsymbol{G}_P''(\boldsymbol{c},\boldsymbol{V})]\!]\|_F^2, \tag{24}$$

where the columns of $\boldsymbol{G}_P''$ are expressed as polynomials using the coefficients $\boldsymbol{c}$ and the Vandermonde matrices based on all the z_i (hence the dependence on $\boldsymbol{V}$ given $z_i = \boldsymbol{v}_i^{\mathrm{T}} \boldsymbol{x}$). The optimisation problem is solved using a quasi-Newton algorithm.

The obtained estimate of $\boldsymbol{V}$ is then used to initialise a final optimisation based on the simulated training output of the decoupled model

$$\arg\min_{\boldsymbol{V},\boldsymbol{c}} \sum_{k=1}^{N_T} (y[k] - y_s[k](\boldsymbol{V},\boldsymbol{c}))^2. \tag{25}$$

Starting from the reference model of Section 3.1, the structured Hessian method is used to obtain a decoupled P-NARX model. The exact same data and operating points are used for fair comparison.
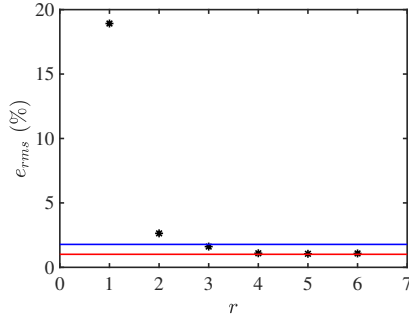
Fig. 6. Black markers: Relative simulation error of the decoupled P-NARX models, computed on the validation data. Red: error obtained from the reference P-NARX model. Blue: error of the $r = 4$ model obtained from the structured Hessian method.

A decoupled P-NARX model with $r = 4$ functions is obtained. Also here polynomials of the third degree are used. The obtained model is of an identical architecture as the $r = 4$ model obtained in Section 3.2, i.e. when considering the $\boldsymbol{w}$ vector to be incorporated in $\boldsymbol{g}$. In Fig. 6, the performance of the decoupled model is compared to the models obtained in Section 3.2. The decoupled model has a slightly higher error of $e_{\mathrm{rms}} = 1.78\%$.

A number of advantages and disadvantages of both methods are listed:

- The structured Hessian method requires the expensive computation of the Hessian.
- The F-CPD method requires a search over the hyperparameter λ.
- The structured Hessian method enforces polynomial constraints on one of the factors. This may be inappropriate when facing non-polynomial nonlinearities.
- The structured Hessian method retrieves an estimate of the factor $\boldsymbol{V}$ from the constrained CPD of the Hessian. The Hessian, however, no longer contains information on the linear part of the NARX model.

5. CONCLUSION

In this work a filtered CPD is used to decouple single-output polynomial NARX models. Polynomial NARX models typically require a large number of parameters in their description. For decoupled structures, the number of parameters grows linearly with the degree, resulting in a substantial model reduction. It was shown that the filtered CPD method no longer relies on the uniqueness properties of the CPD. As a result, the number of univariate functions in the decoupled structure has become a design choice. The method is illustrated on the benchmark problem of the forced Duffing oscillator and compared to the results obtained from the structured Hessian method.

REFERENCES

Billings, S. (2013). *Nonlinear System Identification: NAR-MAX Methods in the Time, Frequency and Spatio-Temporal Domains*. Wiley.

Chan, R., Yuen, J., Lee, E., and Arashpour, M. (2015). Application of nonlinear-autoregressive-exogenous model to predict the hysteretic behaviour of passive control systems. *Eng. Struct.*, 85, 1–10.

Decuyper, J., Dreesen, P., Schoukens, J., Runacres, M., and Tiels, K. (2019). Decoupling multivariate polynomials for nonlinear state-space models. *IEEE Control Systems Letters*, 3(3), 745–750.

Decuyper, J., Tiels, K., Runacres, M.C., and Schoukens, J. (2021a). Retrieving highly structured models starting from black-box nonlinear state-space models using polynomial decoupling. *Mechanical Systems And Signal Processing*, 146.

Decuyper, J., Tiels, K., Weiland, S., and Schoukens, J. (2021b). Decoupling multivariate functions using a nonparametric Filtered-CPD approach. In *IFAC Symposium on System Identification: learning models for decision and control*. Padova, Italy.

Dreesen, P., Ishteva, M., and Schoukens, J. (2015). Decoupling multivariate polynomials using first-order information. *SIAM Journal on Matrix Analysis and Applications*, 36(2), 864–879.

Goodwin, G.C., Aguero, J.C., Cea Garridos, M.E., Salgado, M.E., and Yuz, J.I. (2013). Sampling and sampled-data models: The interface between the continuous world and digital algorithms. *IEEE Control Systems Magazine*, 33(5), 34–53. doi: 10.1109/MCS.2013.2270403.

Karami, K., Westwick, D., and Schoukens, J. (2021). Applying polynomial decoupling methods to the polynomial NARX model. *Mechanical Systems And Signal Processing*, 148.

Karami, K., Westwick, D., and Schoukens, J. (2019). Identification of decoupled polynomial narx model using simulation error minimization* supported by the natural sciences and engineering research council of canada (nserc) through grant rgpin/06464-2015. In *2019 American Control Conference (ACC)*, 4362–4367. doi: 10.23919/ACC.2019.8815172.

Kolda, T.G. and Bader, B.W. (2009). Tensor decomposition and applications. *SIAM Rev.*, 51(3), 455–500.

Levenberg, K. (1944). A method for the solution of certain non-linear problems in least squares. *Quarterly of Applied Mathematics*, 2(2), 164–168.

Schoukens, J., Westwick, D., Ljung, L., and Dobrowiecki, T. (2021). Nonlinear system identification with dominating output noise - a case study on the Silverbox. In *IFAC Symposium on System Identification: learning models for decision and control*.

Westwick, D., Hollander, G., Karami, K., and Schoukens, J. (2018). Using decoupling methods to reduce polynomial NARX models. In *18th IFAC Symposium on System Identification*. Stockholm, Sweden.

Wigren, T. and Schoukens, J. (2013). Three free data sets for development and benchmarking in nonlinear system identification. In *European Control Conference (ECC)*, 2933–2938. Zurich, Switzerland.

Zhao, Y., Billings, S., Wei, H., He, F., and Sarrigiannis, P. (2013). A new NARX-based Granger linear and nonlinear casual influence detection method with application to EEG data. *J. Neurosci. Methods*, 212(1), 79–86.